

Supporting Information

Combined fluorescent and electron microscopic imaging unveils the specific properties of two classes of meiotic crossovers

Lorinda K. Anderson^{*}, Leslie D. Lohmiller^{*}, Xiaomin Tang^{*}, D. Boyd Hammond^{*}, Lauren Javernick^{*}, Lindsay Shearer^{*}, Sayantani Basu-Roy[§], Olivier C. Martin[§], and Matthieu Falque[§]

^{*}Department of Biology, Colorado State University, Fort Collins, CO 80523-1878

[§]INRA, UMR 0320 / UMR 8120 Génétique Végétale, F-91190 Gif-sur-Yvette, France

SI Index: Supporting information for this manuscript includes the following items:

- 1) SI Materials and Methods with Nuclei Selection Criteria and References
- 2) Fig. S1. Set of tomato SCs illustrated in Figure 1
- 3) Fig. S2. SC set immunolabeled with anti-MUS81
- 4) Fig. S3. Individual value plot of RN frequency per nucleus
- 5) Fig. S4. Individual value plot of chiasma patterns and frequencies
- 6) Fig. S5. Scatterplot of length and width for tomato RNs
- 7) Fig. S6. Relationship of RN frequency and SC length
- 8) Fig. S7. BAC-FISH on tomato zygotene SC spreads
- 9) Fig. S8. Comparison of RN frequencies to Poisson distributions
- 10) Fig. S9. Plot of interference strength and fraction P2 COs
- 11) Fig. S10. Distribution of SC distances between pairs of class I – class II COs
- 12) Fig. S11. Same as Fig. S10 but for genetic distances
- 13) Fig. S12. Distribution of SC distances between pairs of class I – class I COs
- 14) Fig. S13. Same as Fig. S12 but for genetic distances
- 15) Table S1. Morphological characteristics and average frequency of RNs for tomato SCs
- 16) Table S2. Morphological characteristics of SCs 5/12 and 7/9
- 17) Table S3. Frequency of SCs with different numbers of MLH1+ and MLH1- RNs
- 18) Table S4. Size and density of RNs
- 19) Table S5. Frequency of RNs in pericentric heterochromatin
- 20) Table S6. Frequency of RNs on short arms of chromosomes
- 21) Table S7. Synaptic patterns for three chromosomes
- 22) Table S8. Analysis of crossover interference
- 23) Table S9. Test of independence between RN numbers on the same SC
- 24) Table S10. Linear regression analysis of RN numbers on the same SC
- 25) Table S11. Test for independence of the two pathways
- 26) Table S12. Inter-crossover distances between P1-P1 COs and between P1-P2 COs

SI Materials and Methods:

SC spreading & Immunolabeling: Primary microsporocytes in pachytene from the highly inbred cherry tomato line (LA4444) were used to prepare SC spreads as described in (1, 2). In brief, protoplasts were mixed with a dilute detergent solution on microscope slides that had been coated with 0.6% Falcon plastic. After nuclei swelled and burst to produce SC spreads, the slides were air-dried for two hours, then stored at -80° for up to two months before immunolabeling. After thawing, slides were treated at room temperature for 10 min with DNase I (1 μ g/ml in 10 mM Tris-HCl, 2.5 mM MgCl₂, 5.0 mM CaCl₂, pH 7.5), washed, then immunolabeled with affinity-purified chicken anti-SISMC1 diluted 1:50 and affinity-purified rabbit anti-SIMLH1 diluted 1:50 (1-4) followed by goat anti-chicken Dylight 649 and goat anti-rabbit AlexaFluor 488 (both from Jackson Labs and diluted 1:500). Primary antibody incubations were performed overnight at 4°C, and secondary antibody incubations were performed at 37°C for one hour. Coverglasses were mounted with Vectashield (Vector Labs) and visualized by fluorescence with a 100X Plan-Apo objective with an adjustable iris and a Leica DM5000 microscope equipped for both phase contrast and fluorescence microscopy with narrow band-pass fluorescein iso-thiocyanate (FITC) and tetramethylrhodamine iso-thiocyanate (TRITC) filter cubes and zero pixel shift.

Fluorescence LM: Using an automated stage (Prior), coordinates for SC spreads were recorded. Red and green signals for each spread were captured individually using a cooled Hamamatsu monochrome 1344X1044 pixel camera and IP Lab software (ver 4). Because some MLH1 foci were quite small and dim, we used long exposure times to be sure that even dim foci would be imaged. Images for each spread were artificially colored using IPLab and merged using Photoshop CS2.

EM: After LM images were captured, the cover glass on each slide was removed by placing the slides in a Coplin jar containing an aqueous solution of 0.05% Triton X-100, 150 mM NaCl, and 50 mM Tris (pH 7.5; TBST). After 10-15 min, the cover glasses were loose enough that each could be gently removed from the slide. Slides were then placed into TBST in a Coplin jar and washed 3 x 5 min with TBST. Slides were given a final wash in deionized water, placed into a slide rack, air-dried, and covered with a 25X50 mm coverglass. Then, using previously recorded coordinates, each SC spread that had at least nine SCs with distinct MLH1 foci was re-imaged by phase microscopy using a 40X objective and a 2X magnifier inserted before the camera. Cover glasses were removed, avoiding damaging the plastic surface, and the slides were stained with phosphotungstic acid (1). After drying, 50-mesh copper finder grids (GC50 – Ted Pella) were placed over as many of the previously imaged SC spreads as possible using phase microscopy to visualize SC spreads. Previously captured phase images aided identification of SC spreads for grid placement. The plastic around the grids was scored with a sharp probe, and then the plastic with grids was lifted from the surface of the slide using 1% hydrofluoric acid followed by 5% acetic acid. Grids with attached plastic were floated onto a distilled water surface where the grids were picked up using small strips of Parafilm (1) and air-dried. Grid coordinates of each SC spread were recorded for examination by EM. SC spreads were photographed at a magnification of 3000X (generally requiring 3 – 6 images each) using a JEOL 2000 EM.

LM-EM image analysis: EM negatives were scanned at 800 dpi using an Epson Perfection V700 Photo scanner. A montage of each SC spread was assembled by hand using

separate layers in Adobe Photoshop CS2. We used Microsoft ICE with Planar Motion 1 to assemble montages for publication. For each EM montage, RNs were identified based on their association with SCs, size (around 50-100 nm), staining (more dense than lateral elements), and fuzzy margins (in contrast to stain precipitate that has sharp margins) (2), and the positions of RNs and kinetochores were marked. The corresponding fluorescent image was pasted as a separate layer over the 800 dpi EM montage, and the size and rotation of the LM image was adjusted as necessary to fit over the EM image. Enhancement of EM or LM images to increase contrast was done uniformly to the entire LM or EM image using the Photoshop “levels” command. While matching the sizes of the LM and EM images was straightforward, matching the rotation was more difficult because the position of each SC spread on each grid as well as the rotation of the grid in the EM holder differed. Therefore, the LM and EM images often were not perfectly matched for every SC. Consequently, each SC was analyzed individually by precisely aligning the red (SC) and green (MLH1) combined fluorescent image over the EM image of the same SC. Then, the MLH1 fluorescent signal at each previously identified RN position was assessed. Each “unlabeled” RN was then more carefully evaluated using only the green channel (instead of the red and green combined image), and any RNs that corresponded to a dim green MLH1 signal were also marked as MLH1-positive RNs. When no green signal could be observed under these conditions (including additional temporary enhancement of the green signal), the RN was marked as an MLH1-negative RN. Kinetochores, MLH1-positive RNs, MLH1-negative RNs, and MLH1 foci on SCs that did not correspond to RNs were marked and their positions on each SC measured using MicroMeasure 3.0

(<http://www.colostate.edu/Depts/Biology/MicroMeasure/>). The image resolution of the bitmap file was adjusted to 200 dpi so the files were not too large to be processed by the MicroMeasure program. After measurement, the chromosome identification of each SC was determined using relative length and arm ratio (Table S1). Occasionally, one or more SCs in a set had to be excluded due to a lack of distinct kinetochores or to the presence of stain precipitate at the EM level that partially obscured SCs. SCs from these groups were used for counting the number of RNs per SC set but were not used for mapping RN positions. Positions of RNs on SCs were measured as a percentage of the arm length from the kinetochore (3). Each RN position was converted to a μm position on the appropriate chromosome using average arm lengths [Table S1, (3)]. Data on RN positions for each SC were combined into an Excel spreadsheet for analysis (Dataset 1).

RN Density: Density measurements of lateral elements, MLH1-negative RNs, and MLH1-positive RNs were taken from 800 dpi EM images using Image J after correcting for background.

Fluorescence *in situ* hybridization (FISH) on zygotene SC spreads: SC spreads from tomato primary microsporocytes in the zygotene stage of meiosis were prepared as described above on uncoated glass slides. FISH was performed as described in (3) using biotin and digoxigenin labeled DNA probes from bacterial artificial chromosomes (BACs). The BACs used were LE_HBa0116C14 (located at 85% of the arm length from the kinetochore on the short arm of chromosome 9); SL_MboI0037108 (located at 95% of the arm length from the kinetochore on the long arm of chromosome 9); LE_HBa0176H22 (located at 87% of the arm length from the kinetochore on the short arm of chromosome 10); LE_HBa0013B20 (located at 96% of the arm length from the kinetochore on the long arm of chromosome 10); LE_HBa0045N22 (located at 97% of the arm length from the kinetochore on the short arm of

chromosome 12); LE_HBa0030J22 (located at 99% of the arm length from the kinetochore on the long arm of chromosome 12) (http://solgenomics.net/cview/map.pl?map_id=13).

Hybridized biotin-labeled probes were detected using consecutive antibody labeling of mouse anti-biotin (1:50), biotinylated donkey anti-mouse (1:100) and streptavidin-5-(4,6-dichlorotriazinyl)aminofluorescein (DTAF; 1:100) and hybridized digoxigenin-labeled probes were detected using consecutive antibody labeling with sheep anti-digoxigenin (1:125) and donkey anti-sheep tetramethylrhodamine iso-thiocyanate (TRITC). The microscope system and imaging parameters were the same as those used for the SC and MLH1 focus imaging (above). All antibodies were from Jackson ImmunoResearch Labs except sheep anti-digoxigenin that was from Roche.

Interference modeling and parameter inference

Generalities

In genetic coordinates, the recombination rate (in mean number of COs per Morgan for a bivalent) is constant and equals 2, allowing for a simpler starting point for further analyses since *CO densities are uniform*. In effect, all the complexity of recombination landscapes becomes irrelevant. This simplification is especially relevant for interference studies, elucidating why nearly all interference models are formulated in genetic coordinates.

In the absence of interference, COs occur independently and the number of COs then follows a Poisson law of mean twice the total genetic length of the chromosome under consideration (measured in Morgan). When COs do *not* occur independently, one says that there is *CO interference*. This phenomenon is usually interpreted as being the signature of an inhibition mechanism whereby a CO newly formed can restrict (allow fewer than expected or none) further COs from forming in its neighborhood. Thus one way to detect such CO interference is to monitor the distribution of distances between adjacent COs: the presence of interference will reduce the frequency of events at short distances.

The Gamma model of crossover formation

To *model* interference and in particular to quantify it *via* an interference “strength”, two directions have been pursued in the literature. The first consists in considering that the COs form via a mechanistic procedure whereby precursors mature into COs through a competitive process (4, 5). The second directly *parameterizes* the inter-CO distances, taking these distances to be independent, identically-distributed, random variables when measuring distances in cM. In this second direction, modelers use the family of gamma distributions, leading to the Gamma model (6). We work in this framework as it is far more widespread, more convenient to implement and it has been applied to several organisms (10, 11). The gamma distribution is characterized by a

rate parameter ρ and a shape parameter ν :
$$\Gamma(x) = \frac{\rho^\nu x^{\nu-1} e^{-\rho x}}{(\nu-1)!}$$

Here, x is the random variable giving the genetic distance between two adjacent COs (x ranges from 0 to +infinity), ν is any real number greater than 0, $(\nu-1)!$ is the factorial of $(\nu-1)$, that is $1 \times 2 \times 3 \times \dots \times (\nu-1)$, but this expression is generalized to non-integer numbers via the *gamma function*. The rate ρ does not affect the *shape* of the distribution; it provides the overall scale. This scale must be set to have the proper density of COs, which by construction is uniform. In the absence of any interference, one can show that the distribution of distances between adjacent COs is an exponential, so $\nu=1$ corresponds to the no-interference case. As ν

increases from 1 to infinity, the distribution takes on a bell shape whose coefficient of variation decreases monotonically from 1 to 0.

In the Gamma model, the rate ρ is fixed by the fact that the mean density of COs is equal to 2 on the SC. This constraint imposes $\rho = 2 nu$, leaving nu as the only adjustable parameter. Furthermore, following Broman and Weber (7), the likelihood of any realization of COs on an SC can be computed for any value of nu . Then to fit nu to the data, we compute the likelihood of the whole data set (all SCs for a given chromosome number) as the product of likelihoods for each SC. This gives us the likelihood of the data given nu . Maximization of this likelihood is then performed using hill climbing (12, 13). In practice this maximization can be done on a desktop computer using the software CODA (8) previously developed. Confidence intervals are computed using the Fisher information matrix.

Three tests for absence of P1-P2 cross-talk

Given that a presumably non-interfering pathway is believed to coexist with the main CO formation pathway (which is interfering and ZMM-dependent), current modeling frameworks take into account the existence of two pathways by a “sprinkling” approach (9). In these models, the non-interfering pathway (P2) of CO formation is superposed onto the interfering one (P1). One of the core hypotheses of the Gamma-sprinkling model is that the two pathways P1 and P2 are independent. To our knowledge, no previous work has investigated whether there is cross-talk between P1 and P2. Here we develop three tests of independence.

The first test considers the distribution of the *numbers* of MLH1-negative and MLH1-positive RNs arising in SCs and asks whether these numbers are independent. For a given chromosome, let $p^+(m)$ (respectively $p^-(n)$) be the experimental probability of SCs with m MLH1-positive and n MLH1-negative RNs and let $P(m,n)$ be the experimental joint probability of these two numbers. Under the hypothesis H_0 of independent pathways, one would have $P(m,n) = p^+(m) p^-(n)$ up to statistical noise. To determine whether the deviations of $P(m,n)$ from that theoretical average are significant, we apply Fisher's exact test. The starting point there is the experimental contingency table giving the corresponding number of SCs found for each value of the pair (m,n) . Let $M(m)$ (respectively $N(n)$) be the number of SCs having m MLH1-positive RNs (respectively n MLH1-negative RNs); $M(m)$ (respectively $N(n)$) is the sum of the SC numbers in the line “ m ” (respectively column “ n ”) of the contingency table. Under H_0 , one considers all possible contingency tables that have the same $M(m)$ and $N(n)$ as the experimental table. If the entries of a table are $\{T(m,n)\}$, the likelihood of that table is given by

$$L(T) = \prod_m M(m)! \cdot \frac{\prod_n N(n)!}{\prod_m \prod_n T(m,n)!} N!$$

where $k!$ is the factorial of k and N is the total number of SCs. The list of all likelihoods (taken over all contingency tables that are possible under H_0) is then enumerated. If $L(T_E)$ is the likelihood of the experimental table, the p -value for rejecting H_0 is the sum of the $L(T)$ for which $L(T)$ is at most $L(T_E)$. This test is provided by the R function *fisher.test()* and we applied it to data for each chromosome separately. We also wanted to provide a global test based on all of the chromosomes. The R function *fisher.test()* does not handle this situation for which there are multiple T_E s. Furthermore, the number of all possible compatible *sets* of contingency tables is then far too large to be enumerated. Thus we implemented Fisher's exact test by sampling rather than by enumerating the sets of compatible tables. In practice we did so by shuffling the

values of n in the data (keeping the shuffling amongst SCs of the same chromosome) so that they are no longer correlated with the values of m . Each shuffle produces a set of contingency tables, one per chromosome; the log-likelihood of each table is computed using the formula above, and then these quantities are summed to have a total log-likelihood for the whole set. The process is repeated 10^9 times. The p -value is then simply obtained by finding the probability that the shuffled values are at least as small as the experimental value. Note that we tested our program against the function *fisher.test()* for each chromosome separately and found excellent agreement, and as expected when all chromosomes are used in our global test, the p -value obtained is much smaller than that of any of the individual chromosomes.

The second test is based on the distribution of cytological distances in micrometers between each MLH1-positive RN and all MLH1-negative RNs of the same SC. The third test is similar except that cytological distances are replaced by genetic distances. For both of these tests, the distributions are compared to those obtained from the same data set after a shuffling as follows: given the list of all SCs, we produce the corresponding series of MLH1-positive RN positions on the one hand, and series of MLH1-negative RN positions on the other for each of these SCs; then we shuffle the order of the first list while keeping the second one unchanged, thereby removing any statistical association between MLH1-positive RNs and MLH1-negative RNs. This shuffling is in fact the same as the one implemented in the first test, though here we keep track of the CO positions, not just CO numbers. A p -value for the null hypothesis H_0 of independence of the pathways P1 and P2 is then obtained by a chi-squared test of comparison between experimental and shuffled distributions.

Note that these procedures allow one to test for absence of cross-talk between P1 and P2 pathways even if the proportion of class II COs varies along the chromosome, that is if the shape of the recombination landscapes are different for class I and class II COs.

The construction of the distribution of distances between MLH1-positive and MLH1-negative RNs requires some justification. Consider an SC in the data set, say the short arm on the left side and the long arm in the right side, and let Y be the genetic position of one of its MLH1-positive RNs. The set of possible distances between that RN and a MLH1-negative RN is not $[0, L]$ but $[0, L-Y]$ for RNs on the right and $[0, Y]$ for RNs on the left. This constraint must be taken into account when constructing the distribution of distances. In practice, we treat RNs on the left first and then continue the procedure for RNs on the right. Given Y , we change the coordinate system, taking Y to be the origin instead of having the origin at the left side of the chromosome.

In our implementation, we use histograms to represent the distributions of CO-CO distances. First a binning of the range $[0, L]$ is defined using 10 bins. Then for every MLH1-positive RN in our data set, we go to the modified coordinate system (shifted by the corresponding Y). The single meiosis under consideration contributes information to the averaged histogram only in the current range $[0, Y]$ for RNs on the left of Y and $[0, L-Y]$ for RNs on the right of Y . For each associated bin we increment an index i_1 that counts the number of SCs for which the current range overlaps with that bin, indicating that such an SC could potentially contribute events (on the left, then on the right) in that bin. If there are MLH1-negative RNs whose (shifted) positions fall into that bin for this meiosis, we also increment another index i_2 by that number of MLH1-negative RNs. At the end, the ratio i_2/i_1 gives the frequency of MLH1-negative RNs in that bin, while the density of the distribution within that bin is taken as that frequency divided by the length of the bin. A small subtlety arises because the extremities of an SC (at positions $-Y$ and $L-Y$) fall *within* a bin and almost never at its end. To

treat this effect, rather than using a unit increase in the count for that bin we increment i_1 by the fraction of the bin that is covered by the SC. A nice feature of this convention is that the sum over all bins of i_1 is equal to the total number of MLH1-positive RNs times the number of bins.

Distance over which interference acts

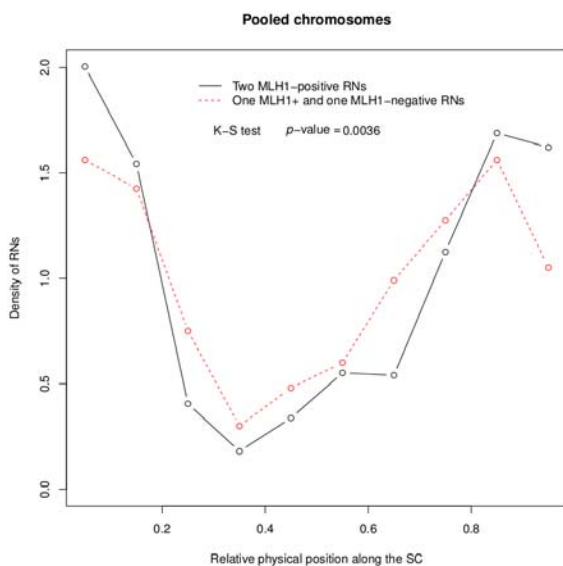
Fig. S10 (respectively S12) displays the distributions (and associated confidence intervals) of inter-CO distances for adjacent pairs of MLH1-positive – MLH1-negative RNs (respectively MLH1-positive – MLH1-positive RNs) for individual chromosomes. The continuous curve in each figure describes the distributions expected without interference. In both cases, the observed distribution falls below the curve at short distances, a feature that leads to the rejection of the hypothesis of no interference, as described above. These distributions can also be used to estimate the physical distance along the SC over which interference acts. We estimated the interference distance as the shortest distance at which the theoretical curve crosses from above to below the observed data (represented by the histogram bar). For the pooled data (see text Fig. 3), the resulting estimate was $\sim 8 \mu\text{m}$ for mixed pairs of MLH-positive and MLH1-negative RNs and $\sim 13 \mu\text{m}$ for pairs of MLH1-positive RNs. When each chromosome is considered separately, the interference distance is consistently higher for pairs of MLH1-positive RNs compared to mixed pairs of MLH1-positive and MLH1-negative RNs (Table S12).

Nuclei selection criteria.

Preliminary experiments showed that some MLH1 foci that corresponded to RNs were quite dim while others were prominent, so nuclei were selected for EM analysis if nine or more SCs had a prominent MLH1 focus. By this criterion, more than a thousand nuclei were selected, and 211 were successfully transferred to grids and analyzed by EM. Of these, 162 had clearly visible RNs and at least one MLH1 focus per SC. These SC sets fulfilled the expected pattern of an obligate CO represented by an MLH1-positive focus on each bivalent [e.g., (1-4)] and were used in this study. Of these 162 nuclei, 150 were complete sets of 12 SCs that were used for evaluating total frequencies of MLH1-positive and MLH1-negative RNs per set, and 132 of the 150 were complete SC sets in which every SC could be identified. The remaining 49 of the original 211 nuclei were not used for the following reasons: the fluorescent image was lost ($n = 1$), the stage of meiosis was too early ($n = 1$), several SCs in the set had extensive asynapsis and/or fragmentation ($n = 4$), the SCs had too much overlying chromatin to be able to identify RNs ($n = 9$) or the nucleus had one or more SCs without an MLH1 focus ($n = 34$). We chose not to use nuclei from the last group because of the high likelihood that these nuclei were inadequately labeled with MLH1 antibodies. For example, MLH1 foci in tomato are variable in size and intensity (10), but the amount of variation (including faint MLH1 foci) that we observed was greater than that shown by (10). Unlike that study, we used DNase I treatment in order to more clearly visualize RNs at the EM level (compare our EM preparations to those of (10) in their Figure 4 and their comments on their inability to identify MLH1-negative RNs), and it is possible that DNase treatment affected detection of MLH1 protein in our preparations. However, with only one exception, all of the SCs without MLH1 foci from the 34 SC spreads had RNs with morphological characteristics like those of MLH1-positive RNs. Using only complete sets of twelve SCs, we compared nuclei that fulfilled the criterion that every SC have an MLH1 focus ($n = 150$) to the nuclei that did not fulfill this criterion ($n = 34$) and found significant differences in the average number of MLH1-positive RNs per set (15.3 and 11.2, respectively, $p < 0.001$) and the average number of MLH1-negative RNs per set (3.5 and 6.8,

respectively, $p < 0.001$) but no significant difference in the average numbers of RNs per set (18.7 and 18.0, respectively, $p > 0.23$). (The 34 nuclei averaged 1.9 SCs per set without an MLH1 focus.) Therefore, we consider it highly likely that SC spreads in which one or more SCs lacked an MLH1 focus represented technical problems with MLH1 immunolabeling, although we cannot exclude the possibility that some RNs contained too little MLH1 protein to detect. Therefore, to minimize the chance that an RN was not labeled with MLH1 antibodies for technical reasons, only *informative* SC sets in which each chromosome had at least one MLH1 focus were selected for measurement and subsequent analysis (Table S3). Using this criterion, we found an average of 15.4 MLH1 foci per nucleus which was similar to the 15.0 MLH1 foci per nucleus reported by (10), indicating that we did not significantly change the number of detectable MLH1 foci by using this approach.

Because of the lack of efficient MUS81 immunolabeling, our interpretation that MLH1-negative RNs mark class II COs cannot be proven directly. As an alternative, we performed a test of the assumption that MLH1-negative RNs are simply cases of failed MLH1 labeling. If this is so, the statistical properties of RN positions on SCs should be independent of whether or not the RNs are MLH1-positive or MLH1-negative. To test this hypothesis, we focused on SCs having two RNs because that's the most frequent situation. We then compared the RN distributions along SCs when both RNs were MLH1-positive to the case when one RN was MLH1-positive and the other was MLH1-negative. Pooling all chromosomes, the Kolmogorov-Smirnoff test led us to reject this hypothesis (p -value = 0.0036; see graph below). Interestingly, the density of RNs is higher at the chromosome extremities for the pairs of MLH1-positive RNs as compared to the mixed pairs of MLH1-positive and MLH1-negative RNs. *A posteriori*, this can be explained because of the stronger interference between Class I COs: having two such COs is unlikely unless they fall near opposite ends of the chromosome. This test thus confirms that the inferred class II crossovers have specific distribution characteristics that are different from those of class I crossovers.



Distribution of RN density on SCs having two RNs. Black solid line: SCs having two MLH1-positive RNs. Red dotted line: SCs having one MLH1-positive RN and one MLH1-negative RN.

References

1. Anderson LK & Stack SM (2013) Preparing SC spreads with RNs for EM analysis. *Plant Meiosis: Methods and Protocols*, eds Pawlowski WP, Grelon M, Armstrong S (Spring Science + Business Media, New York), pp 147-158.
2. Stack SM, Sherman JD, Anderson LK, & Herickhoff LS (1993) Meiotic nodules in vascular plants. *Chromosomes Today*, eds Sumner AT, Chandley AC (Chapman & Hall, London), pp 301-311.
3. Anderson LK *et al.* (2003) High resolution crossover maps for each bivalent of *Zea mays* using recombination nodules. *Genetics* 165:849-865.
4. Kleckner N *et al.* (2004) A mechanical basis for chromosome function. *PNAS USA* 101:12592-12597.
5. King JS & Mortimer RK (1990) A polymerization model of chiasma interference and corresponding computer simulation. *Genetics* 126:1127-1138.
6. McPeck MS & Speed TP (1995) Modeling interference in genetic recombination. *Genetics* 139:1031-1044.
7. Broman KW & Weber JL (2000) Characterization of human crossover interference. *Am. J Hum. Genet.* 66:1911-1926.
8. Gauthier F, Martin OC, Falque M (2011) CODA (crossover distribution analyzer): quantitative characterization of crossover position patterns along chromosomes. *BMC Bioinformatics* 12:27.
9. Copenhaver GP, Housworth EA, Stahl FW (2002) Crossover interference in arabidopsis. *Genetics* 160:1631-1639.
10. Lhuissier FGP *et al.* (2007) The mismatch repair protein MLH1 marks a subset of strongly interfering crossovers in tomato. *Plant Cell* 19:862-876.

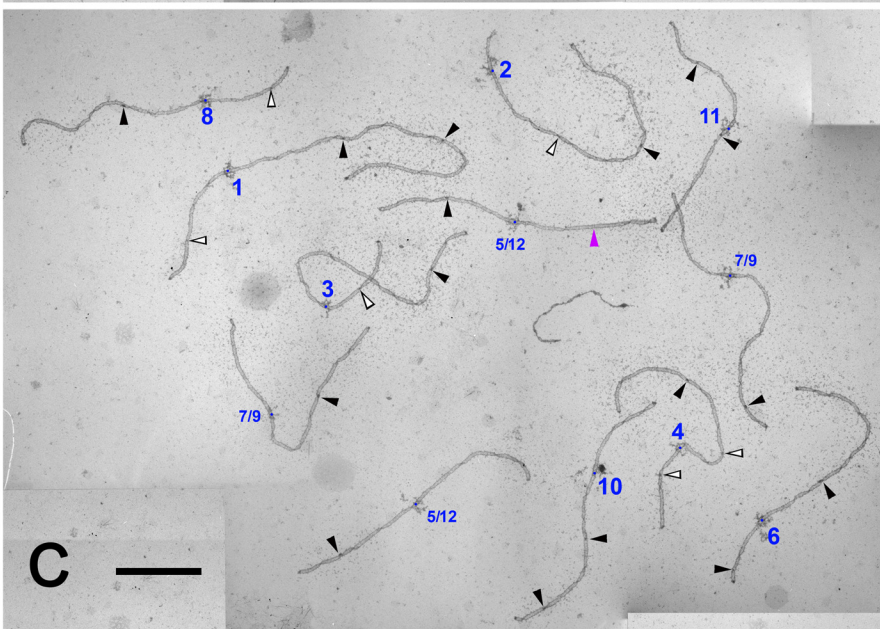
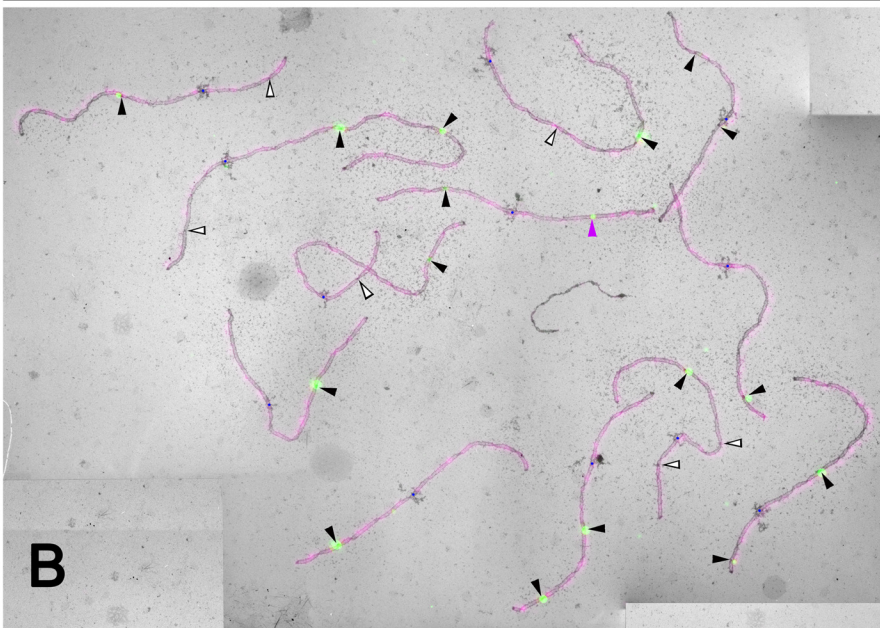
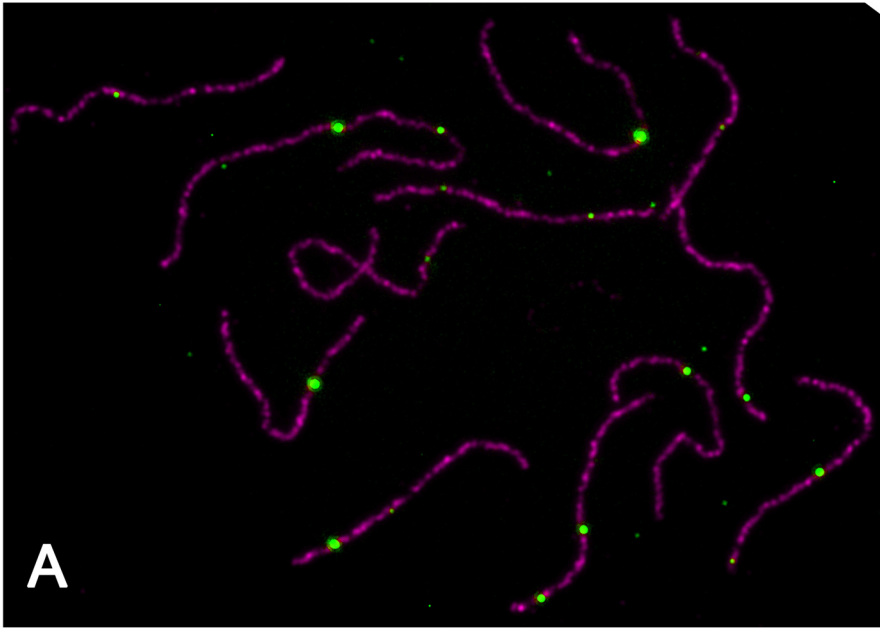


Fig. S1. Set of tomato SCs illustrated in Figure 1. (A) LM fluorescence image showing SCs (magenta) and MLH1 foci (green), (B) fluorescence image superimposed on EM image, and (C) EM image. RNs corresponding to MLH1 foci (MLH1-positive RNs) are indicated by black arrowheads, and RNs that do not correspond to an MLH1 focus (MLH1-negative RNs) are indicated by a white arrow with a black border. One MLH1 focus that does not correspond to an RN (and that likely represents background) is indicated by a magenta arrow in B and C. The kinetochore on each SC is marked by a blue dot and a blue number nearby that identifies the chromosome based on its arm ratio and relative length. SCs 5/12 and SCs 7/9 are morphologically indistinguishable (see Tables S1 and S2). Bar = 5 μ m.

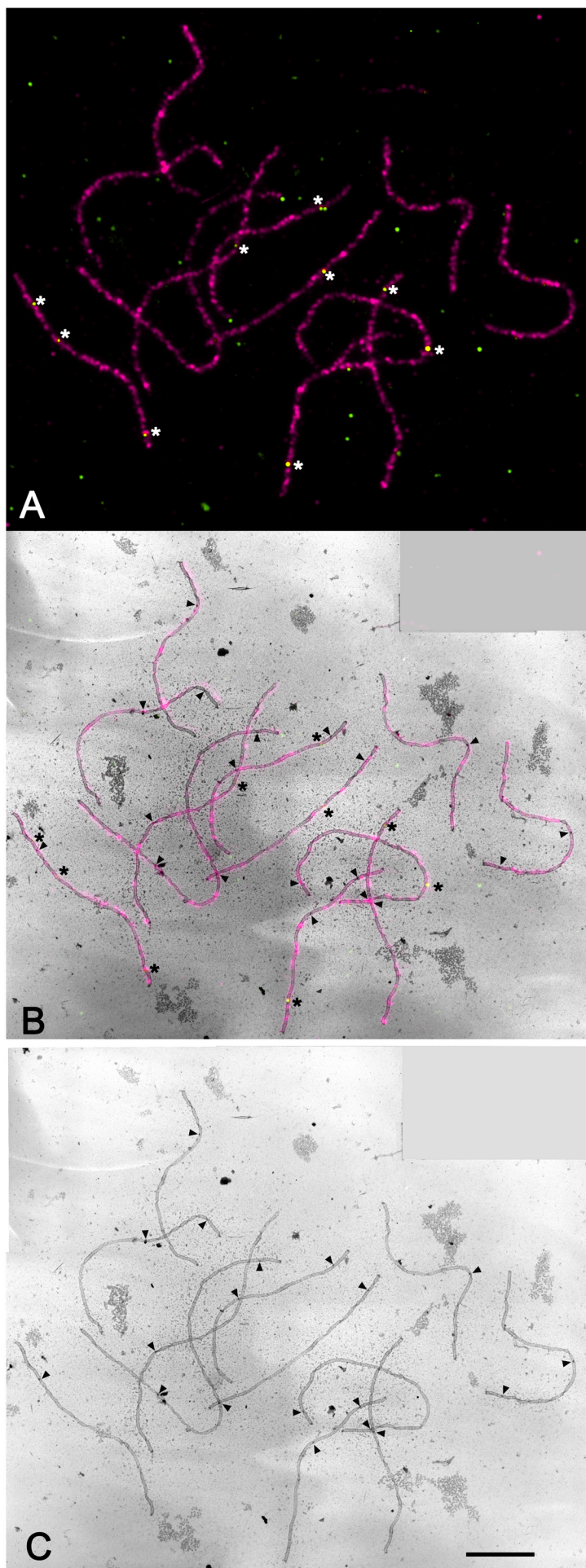


Fig. S2. Light and electron microscopic examination of immunolabeled tomato SCs shows a lack of correspondence of MUS81 foci with RNs. (A) Representative set of tomato SCs immunolabeled with anti-SIMUS81 (green) and anti-SISMC1 (magenta). The locations of MUS81 foci that overlap SCs are indicated by asterisks. (B) Fluorescent image superimposed on EM image of the same SC set. Asterisks indicate MUS81 foci that overlap SCs, and arrowheads indicate locations of RNs. None of the MUS81 foci overlap with an RN. Based on the frequency of MLH1-negative RNs (18%), about 3 of the RNs in this set would have been expected to be labeled with MUS81. (C) EM image of SC spread showing the location of RNs (arrowheads). Among five SC sets of SCs, only 5% (= 5/109) of RNs overlapped a MUS81 focus compared to the expected 19-20 (18%) of MLH1-negative RNs, and the background was high with 95% (= 89/94) of MUS81 foci located on SCs at sites where no obvious morphological structure of any type was present. Essentially the same results were obtained whether using antibodies to Arabidopsis MUS81 protein (graciously provided by James Higgins and Chris Franklin, U. Birmingham) or two different antibodies we developed to the tomato MUS81 protein. Bar = 5 μ m.

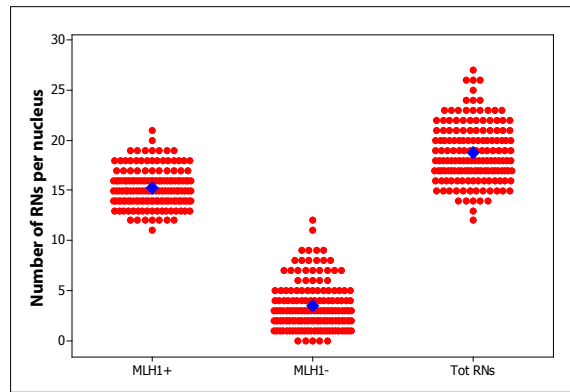


Fig. S3. Individual value plot of RN frequency per nucleus. n=150 sets of 12 SCs. In each distribution, the average number of total (Tot) RNs per nucleus (18.8), the average number of MLH1-positive (MLH1+) RNs per nucleus (15.4), and MLH1-negative (MLH1-) per nucleus (3.4) is indicated by a blue diamond. Each of the nuclei with 11 and 12 MLH1-negative RNs have 15 MLH1-positive RNs.

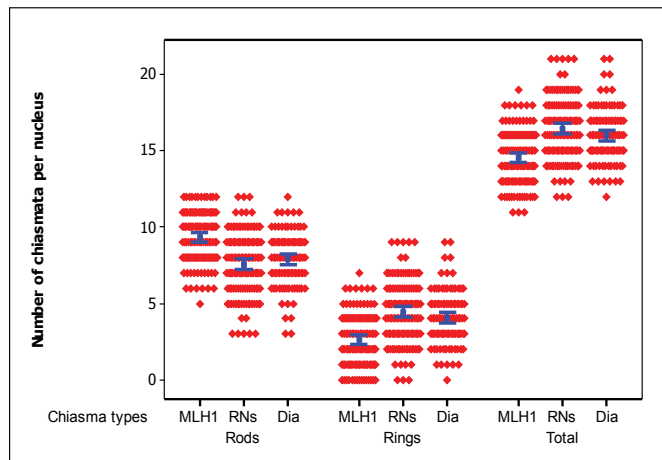


Figure S4. Individual value plot of the number of different chiasma configurations observed from diakinesis chromosomes (Dia) compared to those predicted from RN distribution patterns using only MLH1-positive RNs (MLH1) or using both MLH1-positive and MLH1-negative RNs (RNs). Rods are bivalents with one (or more) chiasma in only one arm and Rings are bivalents with one (or more) chiasma in both arms. To predict chiasma configurations using RNs, each RN was considered to give rise to one chiasma, and one (or more) RN in one arm would be a rod and one (or more) RN in two arms would be a ring. The means of each group are shown with a blue square and the bars represent the 95% confidence limit for each mean. Using only MLH1-positive RNs leads to an over-representation of rods and an under-representation of rings and total chiasmata compared to the observed diakinesis configurations (see Table 1 in text). In comparison, using all RNs give a good match of predicted and observed diakinesis configurations. This indicates that MLH1-negative RNs mark COs that give rise to chiasmata.

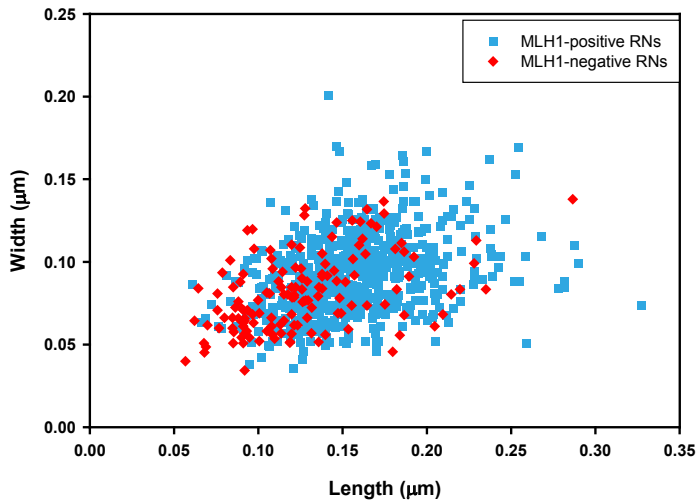


Fig. S5. Scatterplot of length and width for 809 tomato RNs. MLH1-positive RNs (blue squares) are significantly larger (see Table S4) than MLH1-negative RNs (red diamonds) in both length and width, but there is substantial overlap in size between the two RN types.

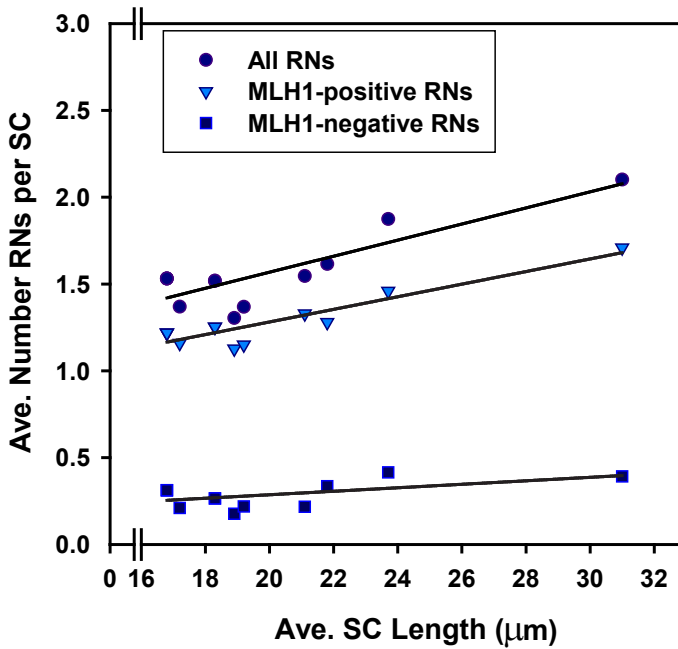


Fig. S6. Relationship between the average number of RNs per SC and average SC length. The frequency of MLH1-negative RNs (boxes) is not strongly correlated with SC length ($y = 0.01x + 0.08$, $r^2 = 0.29$; P slope = 0.07), but the frequency of MLH1-positive RNs (triangles) is significantly positively correlated with SC length ($y = 0.04x + 0.56$, $r^2 = 0.85$; P slope < 0.0001). Because most RNs are MLH1-positive, the relationship for all RNs (circles) and SC length is also positively correlated ($y = 0.05x + 0.64$, $r^2 = 0.73$; P slope = 0.0004).

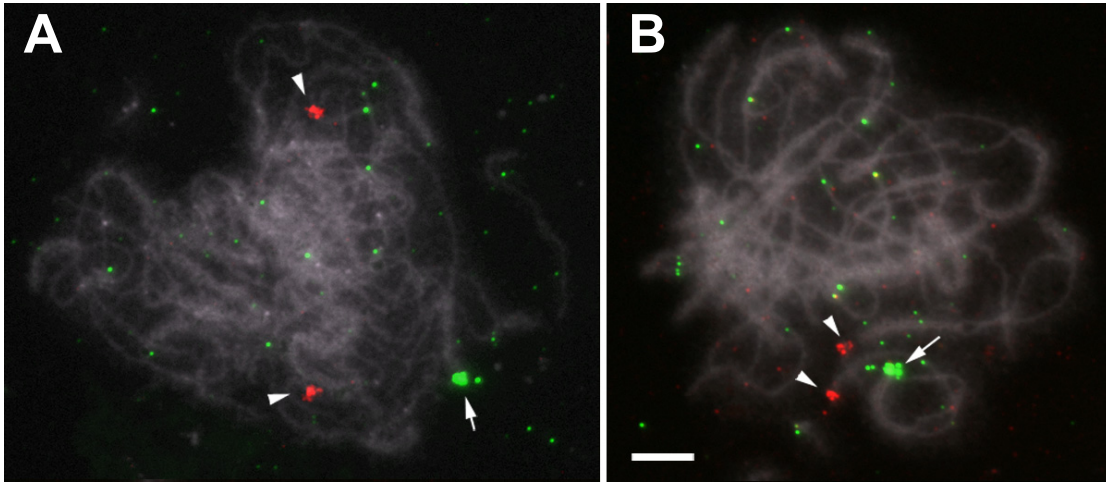
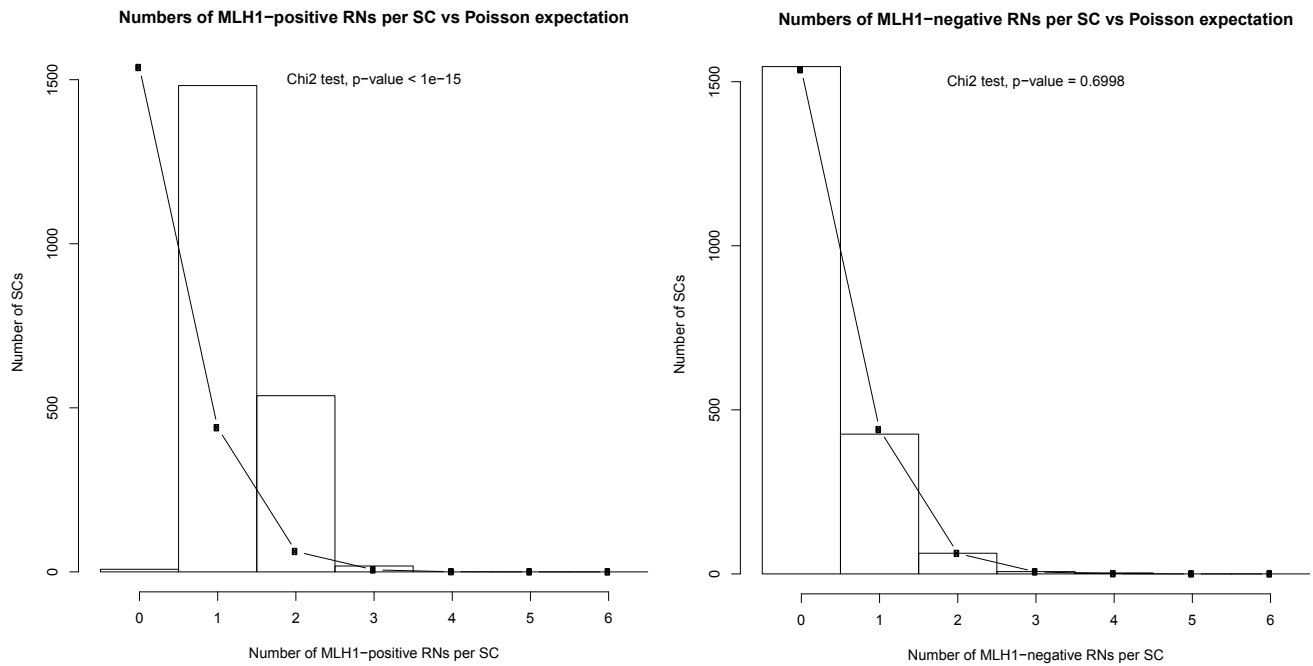


Fig. S7. BAC-FISH on zygotene SC spreads using probes that label the short arms (red; arrowheads) and long arms (green; arrows). (A) acrocentric chromosome 10 and (B) metacentric chromosome 12. Long arms synapse before short arms more often for chromosomes 9, 10 and 12 (Table S7). Bar = 5 μ m.

Fig. S8. Comparison of numbers of MLH1-positive RNs or MLH1-negative RNs per SC compared to Poisson expectations.



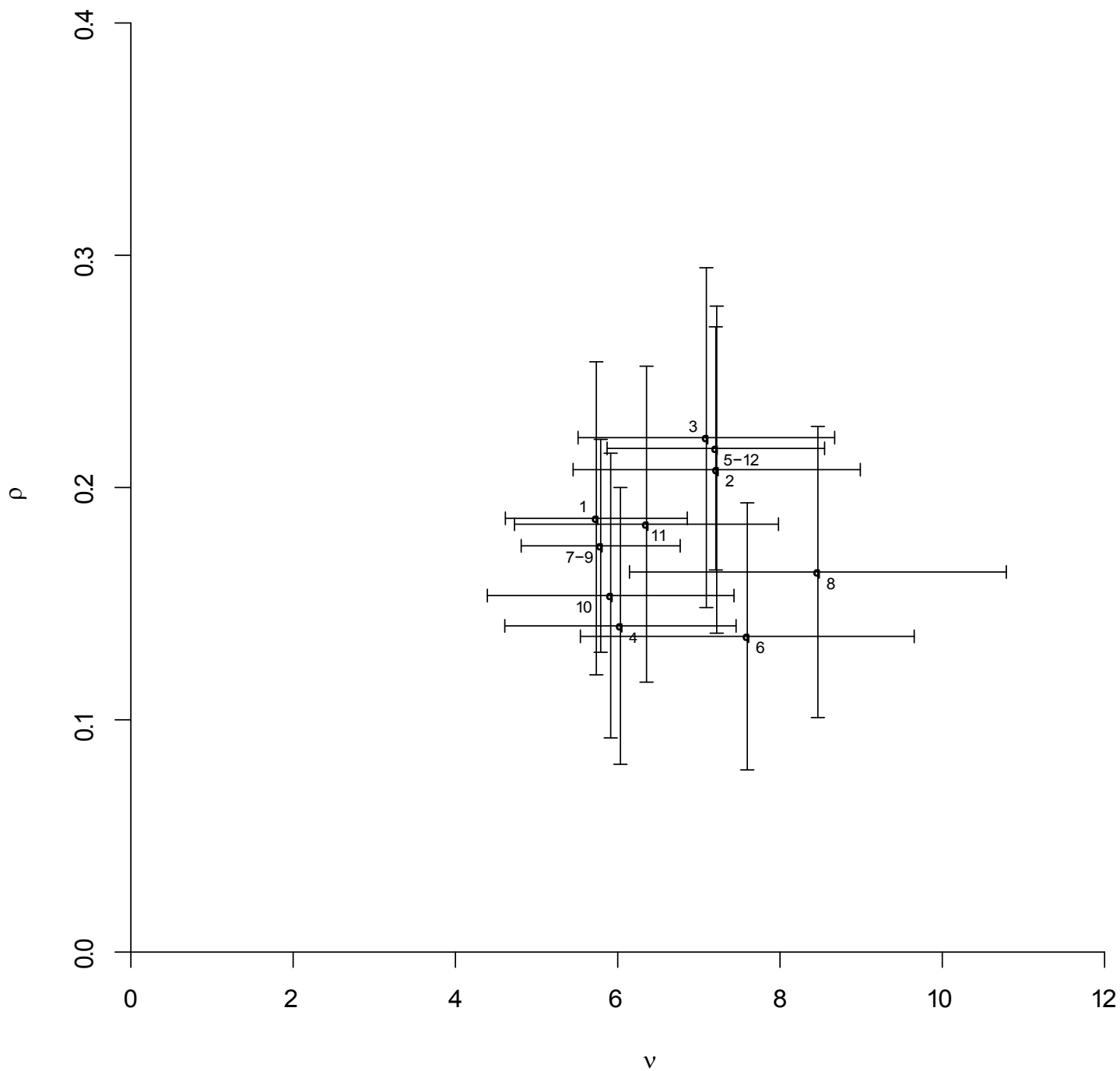


Fig. S9. Interference strength (ν) for MLH1-positive RNs plotted against the proportion of the total RNs represented by MLH1-negative RNs (ρ) for each SC and SC group. The 95% confidence intervals for the estimates of ν and ρ are indicated by horizontal and vertical error bars, respectively.

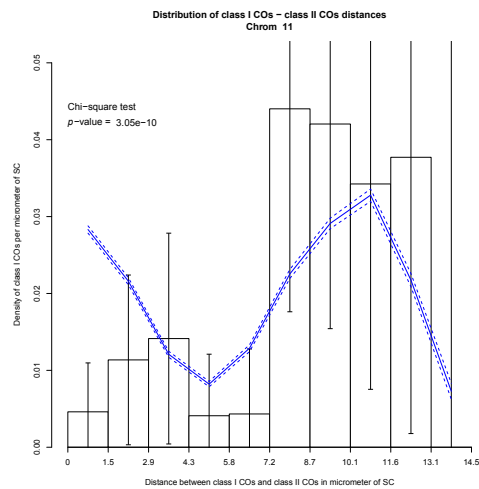
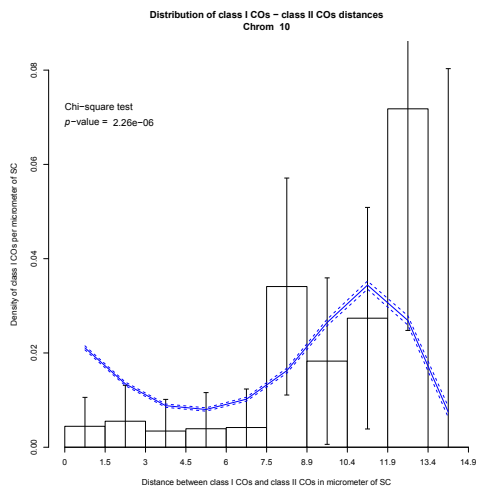
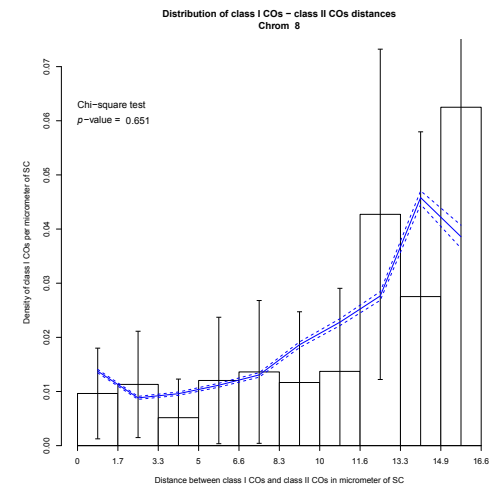
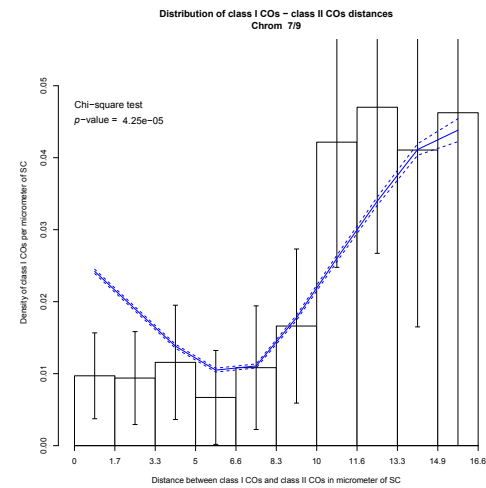
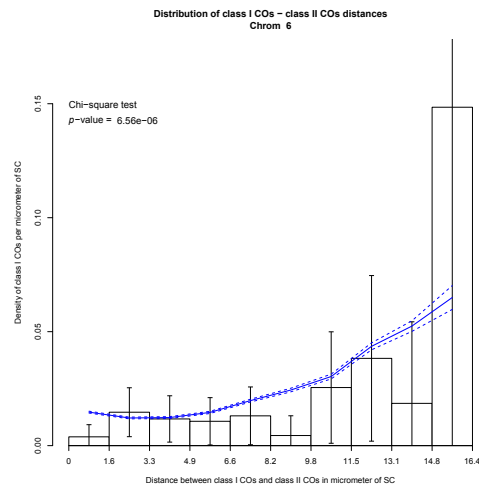
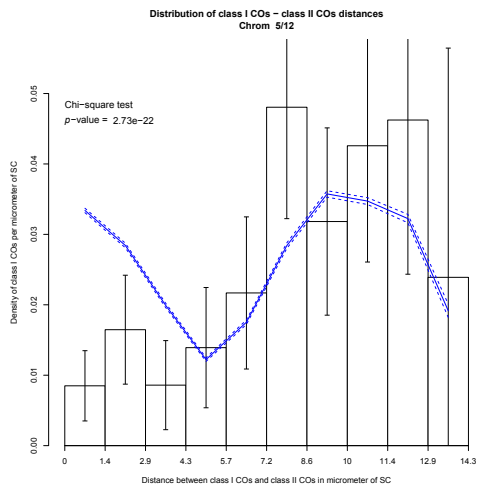
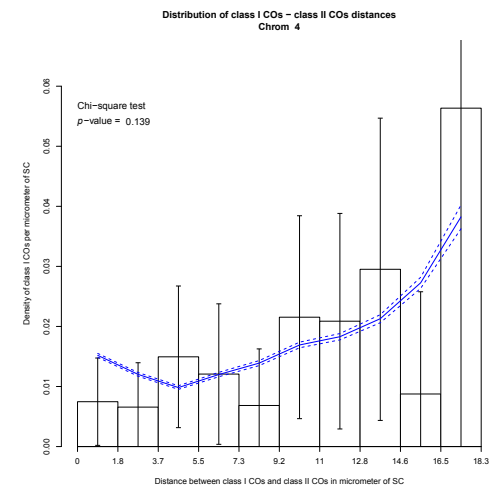
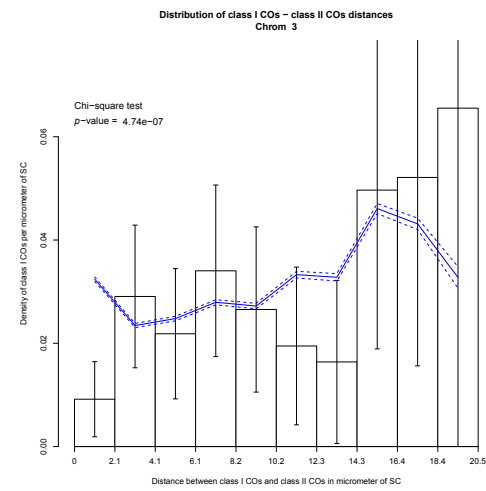
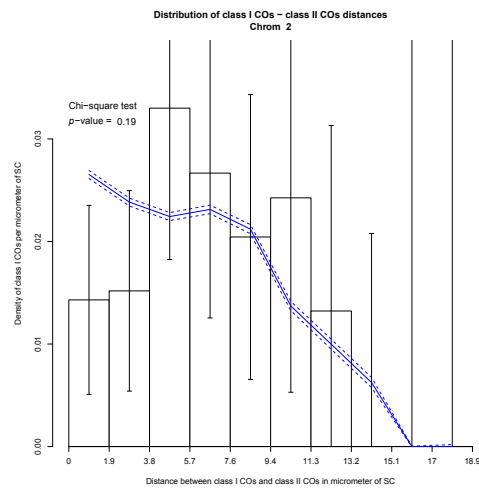
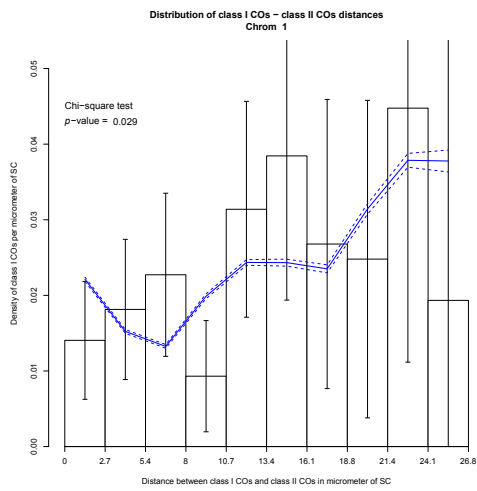


Fig. S10. Distribution of SC distances (μm) between MLH1-positive RNs (class I COs) and MLH1-negative RNs (class II COs) for each individual SC or SC group. Histograms represent the experimental data. Vertical bars represent 95% confidence intervals for each bin of the histogram. The expected distribution in the absence of any cross-talk is plotted as a solid blue line with the associated 95% confidence intervals (dashed blue lines along the solid blue line). Interference between class I and class II COs is indicated by the lower than expected frequency of events at short distances.

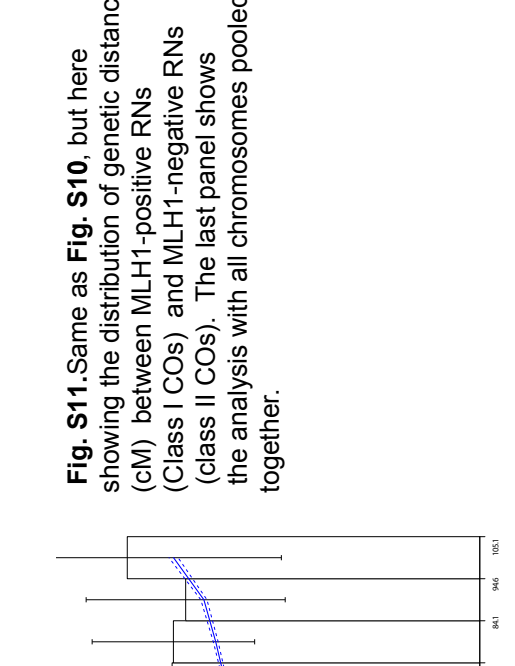
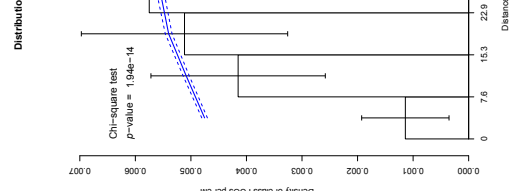
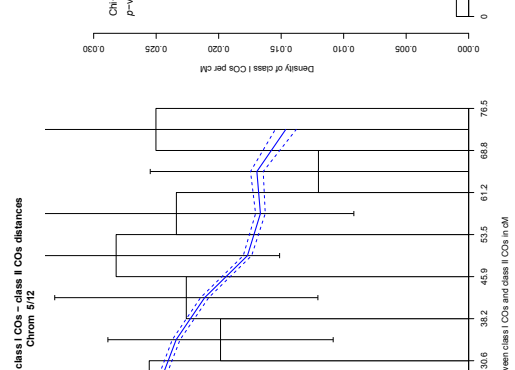
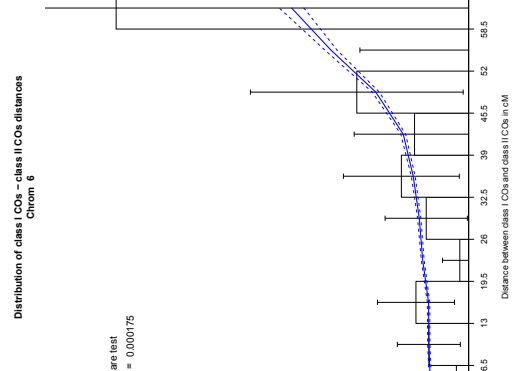
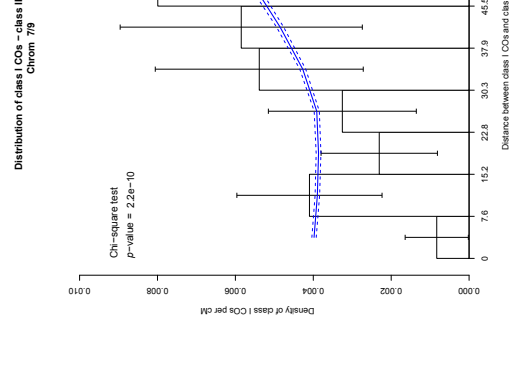
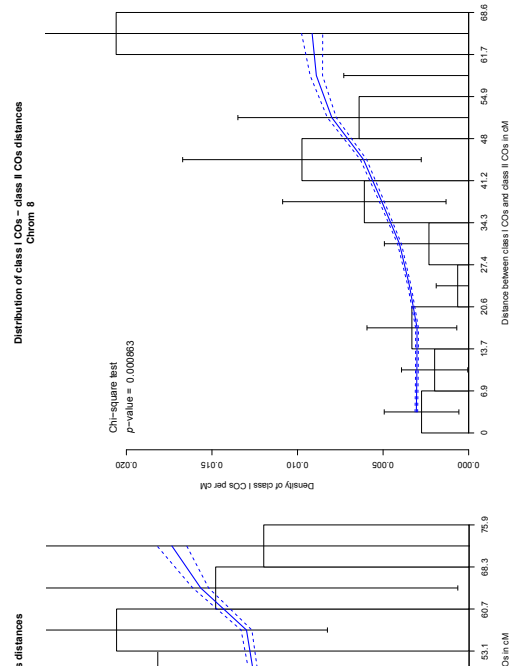
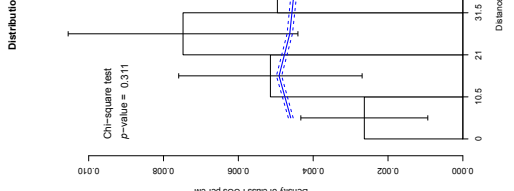
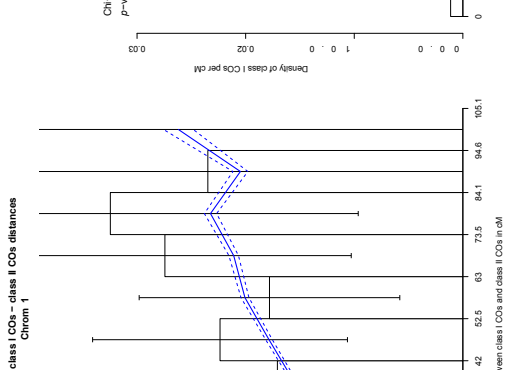
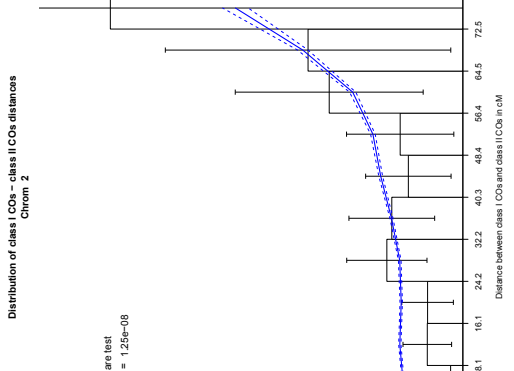
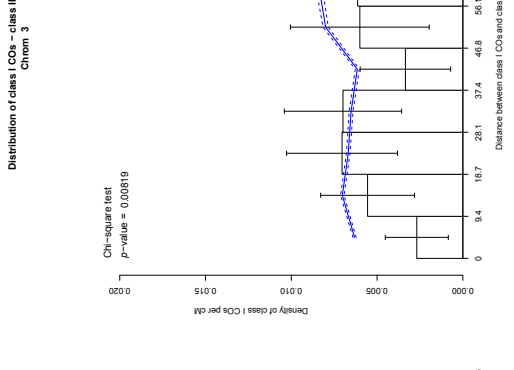
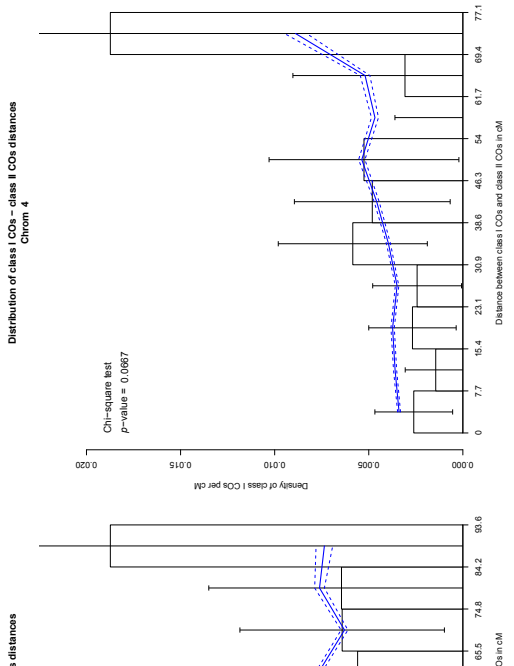


Fig. S11. Same as Fig. S10, but here showing the distribution of genetic distances (cM) between MLH1-positive RNs (Class I COs) and MLH1-negative RNs (class II COs). The last panel shows the analysis with all chromosomes pooled together.

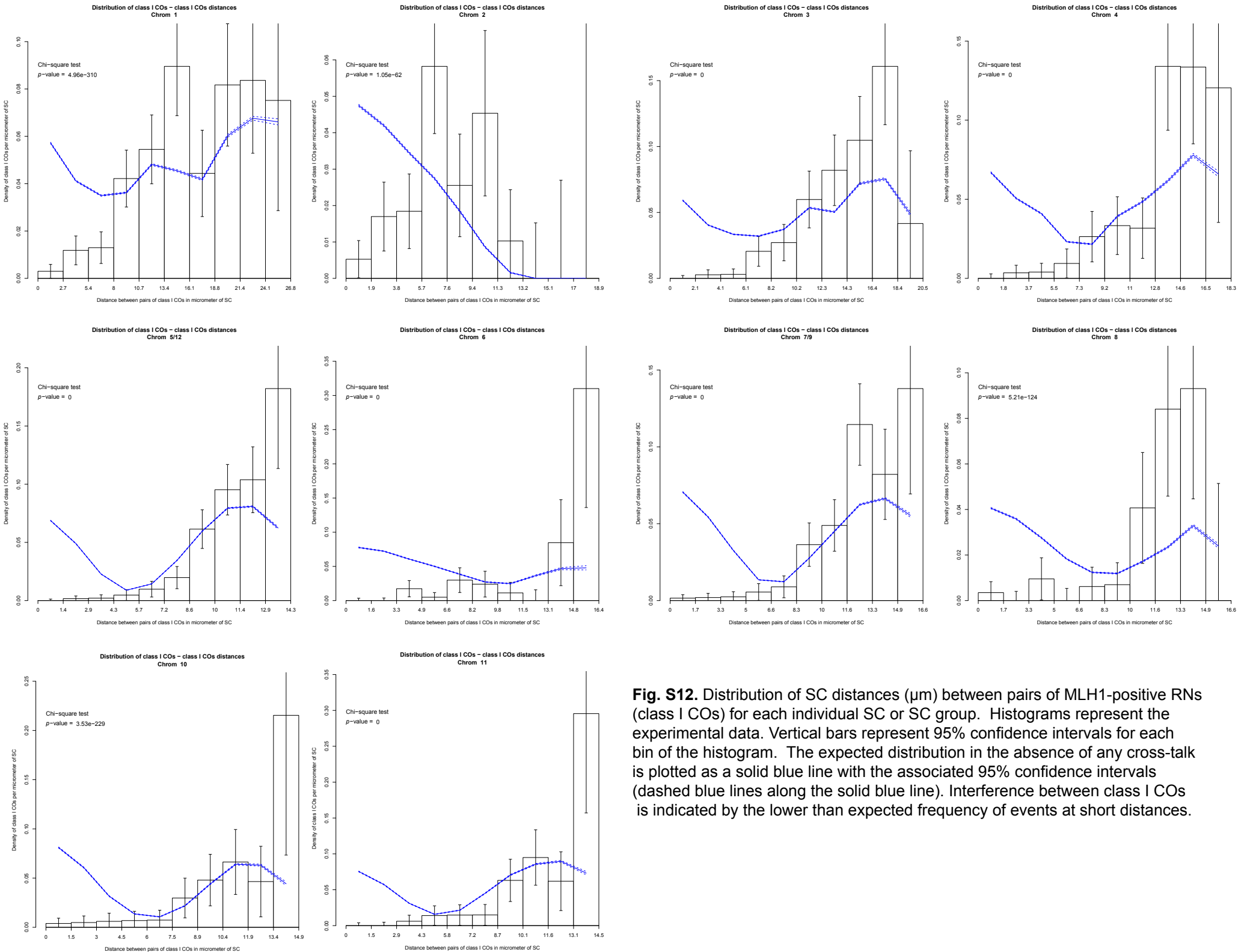


Fig. S12. Distribution of SC distances (μm) between pairs of MLH1-positive RNs (class I COs) for each individual SC or SC group. Histograms represent the experimental data. Vertical bars represent 95% confidence intervals for each bin of the histogram. The expected distribution in the absence of any cross-talk is plotted as a solid blue line with the associated 95% confidence intervals (dashed blue lines along the solid blue line). Interference between class I COs is indicated by the lower than expected frequency of events at short distances.

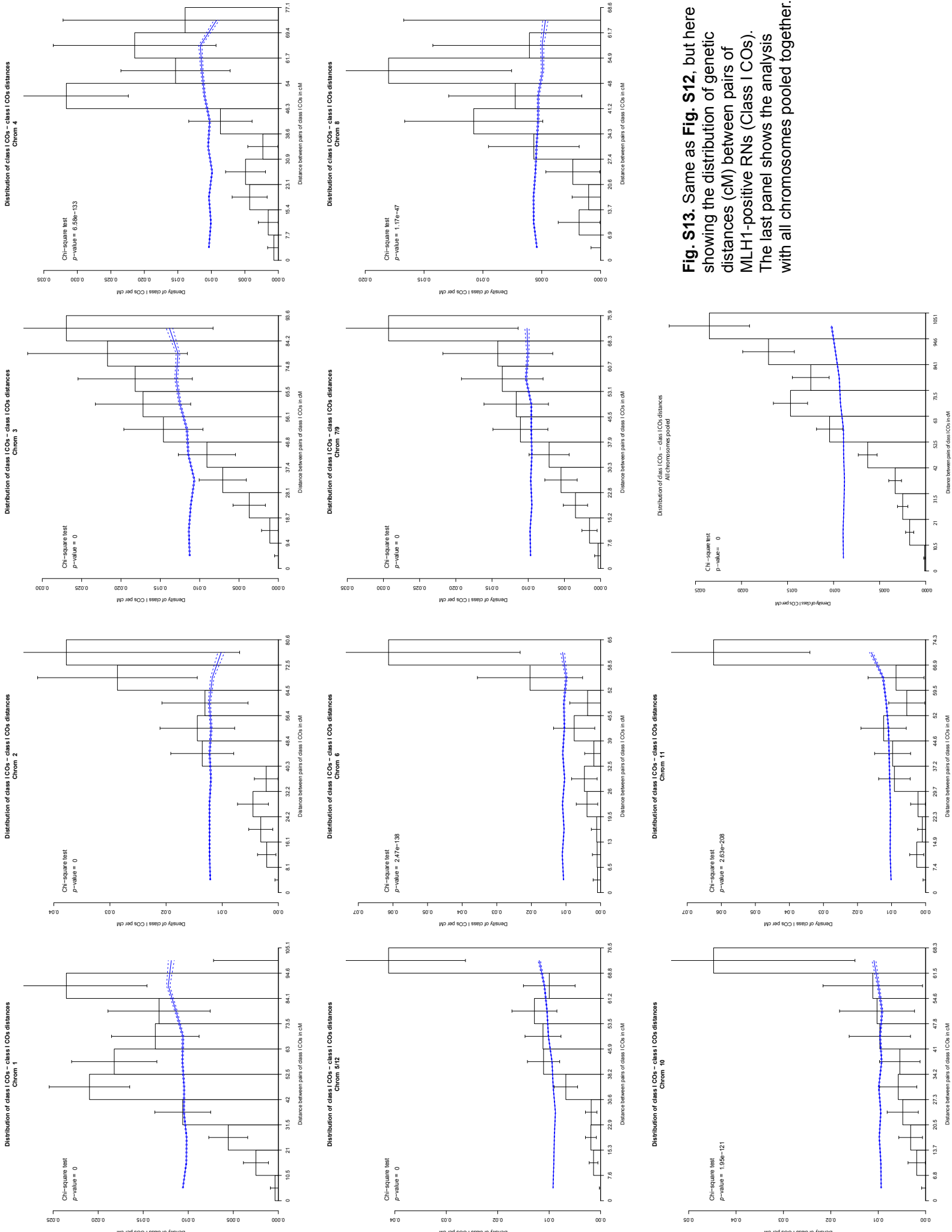


Fig. S13. Same as Fig. S12, but here showing the distribution of genetic distances (cM) between pairs of MLH1-positive RNs (Class I COs). The last panel shows the analysis with all chromosomes pooled together.

Table S1. Morphological characteristics for each of the twelve chromosomes of tomato with the frequencies of MLH1-positive (MLH1+) and MLH1-negative (MLH1-) RNs.

| Chr | μm Length (% of set) ^a | Arm Ratio | Total SCs | Tot. RNs Mean \pm SD | Tot. MLH1+ RNs Mean \pm SD | Tot. MLH1- RNs Mean \pm SD |
|----------------|-------------------------------------------------|--------------|--------------|--------------------------------|------------------------------------|------------------------------------|
| 1 | 31.0 (12.9) | 3.0 | 158 | 332 2.1 \pm 0.84 | 270 1.71 \pm 0.63 | 62 0.39 \pm 0.64 |
| 2 ^a | 21.8 (9.1) | ^a | 161 | 260 1.6 \pm 0.72 | 206 1.28 \pm 0.45 | 54 0.34 \pm 0.61 |
| 3 | 23.7 (9.9) | 3.3 | 159 | 298 1.9 \pm 0.77 | 232 1.46 \pm 0.54 | 66 0.42 \pm 0.66 |
| 4 | 21.1 (8.8) | 2.6 | 152 | 235 1.5 \pm 0.61 | 202 1.33 \pm 0.47 | 33 0.22 \pm 0.47 |
| 5/12 | 17.1 (7.1) | 1.05 | 304 | 475 1.6 \pm 0.63 | 372 1.22 \pm 0.42 | 103 0.34 \pm 0.54 |
| 6 | 18.9 (7.9) | 3.4 | 158 | 206 1.3 \pm 0.58 | 178 1.13 \pm 0.33 | 28 0.18 \pm 0.44 |
| 7/9 | 18.3 (7.6) | 1.8 | 320 | 486 1.5 \pm 0.65 | 401 1.25 \pm 0.45 | 85 0.27 \pm 0.53 |
| 8 | 19.2 (8.0) | 2.4 | 160 | 220 1.4 \pm 0.60 | 184 1.15 \pm 0.36 | 36 0.22 \pm 0.52 |
| 10 | 17.2 (7.2) | 2.1 | 157 | 215 1.4 \pm 0.60 | 182 1.16 \pm 0.42 | 33 0.21 \pm 0.52 |
| 11 | 16.3 (6.8) | 1.2 | 153 | 228 1.5 \pm 0.59 | 186 1.22 \pm 0.43 | 42 0.27 \pm 0.54 |
| Total | 240.0 | | 1882 | 2955 (18.8^b) | 2413 (15.4^c) | 542 (3.4^d) |

^a The short arm of chromosome 2 is usually broken, probably due to the presence of the nucleolus organizer region (1-3), so only the long arm was used for length measurements.

^b Mean number of RNs per nucleus.

^c Mean number of MLH1-positive RNs per nucleus.

^d Mean number of MLH1-negative RNs per nucleus.

1. Sherman JD & Stack SM (1992) Two-dimensional spreads of synaptonemal complexes from solanaceous plants. V. Tomato (*Lycopersicon esculentum*) karyotype and idiogram. *Genome* 35:354-359.
2. Sherman JD & Stack SM (1995) Two-dimensional spreads of synaptonemal complexes from solanaceous plants. VI. High-resolution recombination nodule map for tomato (*Lycopersicon esculentum*). *Genetics* 141:683-708.
3. Lhuissier FGP *et al.* (2007) The mismatch repair protein MLH1 marks a subset of strongly interfering crossovers in tomato. *Plant Cell* 19:862-876.

Table S2. Size characteristics of two pairs of tomato chromosomes that cannot be distinguished based on length and arm ratio.

| Chr | No. obs. | Ave. relative length (SD) | Ave. Arm Ratio (SD) | No. obs. of SA ^a length > LA ^b length (%) |
|----------------|-----------------|------------------------------|------------------------|-----------------------------------------------------------------------|
| 5 | 15 | 7.13 (0.20) | 1.04 (0.03) | 3 (20) ^c |
| 12 | 15 | 7.14 (0.20) | 1.05 (0.03) | 10 (67) ^d |
| <i>t</i> -test | | P > 0.8 | P > 0.3 | |
| 7 | 33 ^e | 7.85 (0.24) | 1.89 (0.10) | NA |
| 9 | 33 | 7.80 (0.25) | 1.91 (0.10) | NA |
| <i>t</i> -test | | P > 0.5 | P > 0.4 | |

Two chromosomes in each of two groups (chromosomes 5 and 12; 7 and 9) are morphologically indistinguishable except by fluorescent in situ hybridization using single-copy probes from bacterial artificial chromosomes (BAC-FISH). Because chromosomes 5 and 12 are nearly perfectly metacentric, BAC-FISH also made it possible to determine how often the short arm of the SC was measured as being longer than the long arm of the SC. Separate BAC-FISH probes were used to identify one arm of chromosome 7 and one arm of chromosome 9 in another group of 33 SC sets. The data presented here are based on LM measurements only, which give slightly different average relative lengths and arm ratios for chromosomes 7 and 9 than we obtained using EM (Table S1).

^a SA = short arm

^b LA = long arm

^c A separate group of 305 SC sets in which one of the two arms of chromosome 5 were identified by FISH showed 74 examples (24%) in which the SA was longer than the LA.

^d A separate group of 325 SC sets in which one of the two arms of chromosome 12 were identified by FISH showed 177 examples (54%) in which the SA was longer than the LA.

^e Twelve of the 33 sets were missing one or more SCs (incomplete SC sets), so n = 21 for relative length values using complete SC sets.

Table S3. Frequency of SCs with different numbers of MLH1-positive and MLH1-negative RNs.

| Chr | Total SCs | Ratio of Number of MLH1-positive RNs : Number of MLH1-negative RNs (% of SCs observed for each class) ^a | | | | | | | | | | |
|-------|-----------|-----------------------------------------------------------------------------------------------------------------------|-------------|-------------|--------------|------------|------------|-------------|-------------|-----------|--------------------|-------------|
| | | 3:0 | 2:0 | 1:0 | ≥1:0 | 3:1 | 2:1 | 1:1 | 2:2-3 | 1:2-4 | 0:1-4 ^b | ≥0:≥1 |
| 1 | 158 | 12 (8) | 56 (35) | 39 (25) | 107 (68) | 3 (2) | 23 (15) | 16 (10) | 3 (2) | 6 (4) | 0 | 48 (30) |
| 2 | 161 | 0 | 36 (22) | 79 (49) | 115 (71) | 0 | 7 (4) | 34 (21) | 2 (1) | 3 (2) | 0 | 46 (29) |
| 3 | 159 | 1 (0.6) | 51 (32) | 53 (33) | 105 (66) | 1 (1) | 16 (10) | 27 (17) | 3 (2) | 6 (4) | 1 (0.6) | 53 (33) |
| 4 | 152 | 0 | 45 (30) | 78 (51) | 123 (81) | 0 | 5 (3) | 20 (13) | 0 | 4 (3) | 0 | 29 (19) |
| 5/12 | 304 | 0 | 57 (19) | 155 (51) | 212 (70) | 0 | 12 (4) | 68 (22) | 0 | 11 (4) | 1 (0.3) | 92 (30) |
| 6 | 158 | 0 | 16 (10) | 118 (75) | 134 (85) | 0 | 2 (1) | 18 (11) | 2 (1) | 2 (1) | 0 | 24 (15) |
| 7/9 | 320 | 0 | 68 (21) | 178 (56) | 246 (77) | 1 (0.3) | 12 (4) | 51 (16) | 0 | 9 (3) | 1 (0.3) | 73 (23) |
| 8 | 160 | 0 | 22 (14) | 108 (68) | 130 (81) | 0 | 2 (1) | 24 (15) | 0 | 4 (3) | 0 | 30 (19) |
| 10 | 157 | 0 | 26 (17) | 103 (66) | 129 (82) | 0 | 2 (1) | 20 (13) | 0 | 3 (2) | 3 (2) | 28 (18) |
| 11 | 153 | 0 | 33 (22) | 85 (56) | 118 (77) | 0 | 1 (0.7) | 27 (18) | 0 | 6 (3) | 1 (0.7) | 35 (23) |
| TOTAL | 1882 | 13 (0.7) | 410 (22) | 997 (53) | 1419 (75) | 5 (0.3) | 82 (4) | 305 (16) | 10 (0.5) | 53 (3) | 7 (0.4) | 463 (25) |

^a Percentages are rounded to nearest integer number, except when < 1%.

^b SCs in this class represent those with a distinct MLH1 focus that did not correspond to an RN. This is because SC sets containing at least one MLH1 focus on each SC (and not necessarily that each MLH1 focus corresponded to an RN) were selected for analysis. These foci presumably represent background foci that are often observed in immunofluorescent preparations. Background foci that did not correspond to RNs were occasionally observed on other SCs also.

Table S4. Size and density of MLH1-positive (MLH1+) and MLH1-negative (MLH1-) RNs.

a. RN size comparison

| RN type | No. obs. | RN length in nm (SD) | RN width in nm (SD) |
|---------|----------------|----------------------|---------------------|
| MLH1+ | 669 | 157 (36) | 93 (24) |
| MLH1- | 140 | 127 (41) | 81 (23) |
| | <i>t</i> -test | $P < 0.001$ | $P < 0.001$ |

b. RN density comparison

| Structure | No. obs. ^a | Mean relative density ^b (SD) | Statistics |
|-----------------|-----------------------|-----------------------------------------|------------------------------------------------------------------------------------|
| MLH1+ | 72 | 91.8 (22.6) | ANOVA, $P = 0.0008$; Tukey simultaneous comparison test, $P \leq 0.0008$ |
| MLH1- | 54 | 78.8 (19.2) | |
| SC ^c | 51 | 54.1 (14.0) | |

^a The RNs used for density comparisons represent a sample of the RNs used for the dimension comparison.

^b Relative density is the density measurement above background as defined using Image J.

^c The SC density measurements represent samples from a lateral element of the SC near the RN that was measured.

Table S5. Frequency of RN types on SC in pericentric heterochromatin. A total of 162 of 2955 (=5%) of RNs were observed in heterochromatin.

| Chr | Eu/Het Borders (% total SC length) ^a | No. MLH1 ⁺ RNs (%) ^b | No. MLH1 ⁻ RNs (%) ^c |
|--------------|----------------------------------------------------|-----------------------------------------------|-----------------------------------------------|
| 1 | 12-40 (28) | 10 (3.7) | 13 (21.0) |
| 2 | 0-36 (36) | 3 (1.5) | 7 (13.0) |
| 3 | 22-44 (22) | 10 (4.3) | 13 (19.7) |
| 4 | 18-48 (30) | 9 (4.5) | 7 (21.2) |
| 5/12 | 38-68 (30) | 9 (2.4) | 14 (13.6) |
| 6 | 12-38 (26) | 6 (3.4) | 5 (17.9) |
| 7/9 | 24-54 (30) | 6 (1.5) | 10 (11.8) |
| 8 | 20-50 (30) | 2 (1.1) | 7 (20.0) |
| 10 | 20-54 (34) | 6 (3.3) | 8 (24.2) |
| 11 | 38-72 (34) | 11 (5.9) | 6 (14.6) |
| Total | (ave = 30%) | 72 (3.0) | 90 (16.6) |

^a Borders expressed as percentage of SC length from the tip of the short arm (see text ref. 32).

^b Percentages calculated using total MLH1-positive (MLH1+) RNs per SC given in Table S1.

^c Percentages calculated using total MLH1-negative (MLH1-) RNs per SC given in Table S1.

Table S6. Comparison of MLH1-positive (MLH1+) and MLH1-negative (MLH1-) RN frequency on the short arms (SA) of tomato chromosomes.

| Chr ^a | Short arm as % of total Chr. Length ^b | % of MLH1+ RNs on short arm (SA#/Tot) | % MLH1- RNs on short arm (SA#/Tot) | <i>p</i> -value ^c MLH1+ RNs | <i>p</i> -value ^c MLH1- RNs |
|------------------|--------------------------------------------------|---------------------------------------|------------------------------------|----------------------------------------|----------------------------------------|
| 1 | 25 | 24 (64/270) | 44 (27/62) | 0.673 | 0.002 |
| 3 | 23 | 31 (72/232) | 36 (24/66) | 0.005 | 0.013 |
| 4 | 28 | 25 (50/202) | 48 (16/33) | 0.347 | 0.012 |
| 5/12 | 49 | 57 (212/372) | 48 (49/103) | 0.002 | 0.844 |
| 6 | 23 | 7 (13/178) | 54 (15/28) | 5.10 ⁻⁸ | 4.10 ⁻⁴ |
| 7/9 | 35 | 25 (100/401) | 48 (41/85) | 2.10 ⁻⁵ | 0.012 |
| 8 | 29 | 14 (25/184) | 56 (20/36) | 1.10 ⁻⁶ | 0.001 |
| 10 | 32 | 21 (39/182) | 55 (18/33) | 0.002 | 0.008 |
| 11 | 45 | 60 (111/186) | 48 (20/42) | 6.10 ⁻⁵ | 0.758 |
| Total | | 28 (686/2413) | 43 (235/542) | | |

^a Because the heterochromatic short arm of chromosome 2 is usually broken, this chromosome is not considered here. In total, we observed five MLH1-negative RNs but no MLH1-positive RNs on the fragmented, heterochromatic short arm of chromosome 2. All of the chromosomes have distinct short arms except chromosomes 11 and 5/12 that are near-metacentrics.

^b Calculated from Table S1.

^c *p*-values for the H_0 hypothesis that the probability that a RN occurs in the short arm is equal to the length of this short arm divided by the total length of the SC. The two-sided *p*-value was obtained by summing the probabilities of all possible outcomes of numbers *n* (of RNs on the short arm) that are at least as unlikely as the one found experimentally. These individual probabilities are equal to the binomial density (function *dbinom*(*n*, *N*, *f*) in R) where *N* is the total number of RNs on the SC, and *f* is the proportion of the SC length covered by the short arm.

Table S7. Frequency of synapsis of long arm compared to short arm for acrocentric chromosomes 9 and 10 and near-metacentric chromosome 12, using BAC-FISH¹ to identify each arm simultaneously in early to mid-zygotene SC spreads.

| Chr | No. obs. ² | Synapsed arm (%) | | Exp. ratio ³ | Obs. ratio ⁴ | <i>p</i> -value ⁵ |
|-----|-----------------------|------------------|---------|-------------------------|-------------------------|------------------------------|
| | | Short | Long | | | |
| 9 | 31 | 7 (23) | 24 (77) | 1.8 | 3.43 | 0.087 |
| 10 | 124 | 25 (20) | 99 (80) | 2.1 | 3.96 | 0.002 |
| 12 | 54 | 24 (44) | 30 (56) | 1.05 | 1.25 | 0.309 |

¹ BAC-FISH - Bacterial artificial chromosome fluorescence in situ hybridization.

² Only informative zygotene sets in which one arm synapsed before the other were used. Sets in which both SC ends were synapsed or unsynapsed were excluded from this analysis.

³ Long arm length divided by short arm length (arm ratio) from Table S1.

⁴ Number of times the long arm synapsed first divided by the number of times the short arm synapsed first.

⁵ *p*-values for the H_0 hypothesis that the probability that synapsis starts on a given arm is equal to the length of this arm divided by the total length of the SC. The *p*-value was given by the R function *pbinom*(*n_{short}*, *N*, *f*) where *n_{short}* is the number of times the short arm synapses first, *N* is the number of FISH observations, and *f* = 1/(1 + *armratio*).

Table S8. Analysis of crossover interference.

| RN type | Chr | ν | 95% CI |
|---------|-------|-------|------------|
| MLH1+ | 1 | 5.7 | 4.6 – 6.9 |
| | 2 | 7.2 | 5.5 – 9.0 |
| | 3 | 7.1 | 5.5 – 8.7 |
| | 4 | 6.0 | 4.6 – 7.5 |
| | 5-12 | 7.2 | 5.9 – 8.5 |
| | 6 | 7.6 | 5.5 – 9.7 |
| | 7-9 | 5.8 | 4.8 – 6.8 |
| | 8 | 8.5 | 6.1 – 10.8 |
| | 10 | 5.9 | 4.4 – 7.4 |
| | 11 | 6.4 | 4.7 – 8.0 |
| | MLH1- | 1 | 1.0 |
| 2 | | 1.0 | 1.0 – 1.5 |
| 3 | | 1.1 | 1.0 – 1.4 |
| 4 | | 1.1 | 1.0 – 1.6 |
| 5-12 | | 1.2 | 1.0 – 1.6 |
| 6 | | 1.0 | 1.0 – 1.5 |
| 7-9 | | 1.0 | 1.0 – 1.2 |
| 8 | | 1.0 | 1.0 – 1.4 |
| 10 | | 1.0 | 1.0 – 1.3 |
| 11 | | 1.0 | 1.0 – 1.7 |

Crossover interference strength parameter ν for MLH1-positive (MLH1+) and MLH1-negative (MLH1-) RNs. For each RN distribution, ν was estimated using a single-pathway Gamma model of interference. The case $\nu = 1$ corresponds to the absence of interference, and increasing values of ν indicate increasing positive interference strength. The 95% confidence interval (95% CI) for each estimated value of ν is computed using Fisher's information matrix.

Table S9. Test of independence between the numbers of MLH1-negative and MLH1-positive RNs on the same SC.

| Chr | 1 | 2 | 3 | 4 | 5/12 | 6 | 7/9 | 8 | 10 | 11 |
|-----------------|------|------|------|------|-------------|------|------|------|------|-------------|
| <i>p</i> -value | 0.70 | 0.13 | 0.03 | 0.12 | 2.10^{-5} | 0.14 | 0.07 | 0.67 | 0.02 | 7.10^{-4} |

p-values of the Fisher's exact test (function *fisher.test()* of R) on each chromosome when considering the H_0 hypothesis that the numbers of MLH1-negative RNs per SC is the same whether the SCs have one, two, or three MLH1-positive RNs. When all chromosomes are pooled, the *p*-value is less than 10^{-9} .

Table S10. Linear regression analysis (function $lm()$ of R) between the number of MLH1-negative RNs and the number of MLH1-positive RNs on the SC for each chromosome.

| Chr | 1 | 2 | 3 | 4 | 5/12 | 6 | 7/9 | 8 | 10 | 11 |
|-----------------|-------|-------|-------|-------|--------------------|-------|-------|-------|-------|--------------------|
| R ² | 0.016 | 0.009 | 0.034 | 0.03 | 0.042 | 0.011 | 0.013 | 0.013 | 0.034 | 0.082 |
| slope | -0.13 | -0.13 | -0.23 | -0.18 | -0.26 | 0.14 | -0.13 | -0.17 | -0.23 | -0.36 |
| <i>p</i> -value | 0.12 | 0.24 | 0.02 | 0.03 | 8.10 ⁻⁶ | 0.19 | 0.04 | 0.15 | 0.02 | 3.10 ⁻⁴ |

p-values correspond to the H_0 hypothesis that the slope of the regression is equal to zero.

Table S11. Test for independence of the two pathways based on SC distances between MLH1-positive and MLH1-negative RNs.

| Chr | 1 | 2 | 3 | 4 | 5/12 | 6 | 7/9 | 8 | 10 | 11 |
|-----------------|-------|-------|--------------------|-------|---------------------|--------------------|--------------------|-------|--------------------|---------------------|
| <i>p</i> -value | 0.029 | 0.190 | 5.10 ⁻⁷ | 0.139 | 3.10 ⁻²² | 7.10 ⁻⁶ | 4.10 ⁻⁵ | 0.651 | 2.10 ⁻⁶ | 3.10 ⁻¹⁰ |

p-values of the chi-square test (function *chisq.test()* of R; see Materials and Methods). When all chromosomes are pooled, the *p*-value is less than 10⁻⁹.

Table S12. Intercrossover distances (μm SC length and fractional SC length) between MLH1-positive (MLH1+) and MLH1-negative (MLH1-) RNs and between pairs of MLH1-positive RNs as defined by the point at which the line describing the frequencies of intercrossover distances expected in the absence of interference overlaps the observed distribution of intercrossover distances for each SC (see Figs. S10 and S12 and nuclei selection criteria section).

| Chr | SC length (μm) | MLH1+ MLH1- interference distance | | MLH1+ MLH1+ interference distance | |
|-----------------|--------------------------------|--------------------------------------|----------|--------------------------------------|----------|
| | | μm | fraction | μm | fraction |
| 1 | 26.8 | 2.7 | 0.10 | 8.0 | 0.30 |
| 2 | 18.9 | 3.8 | 0.20 | 5.7 | 0.30 |
| 3 | 20.5 | 2.1 | 0.10 | 10.2 | 0.50 |
| 4 | 18.3 | 3.7 | 0.20 | 7.3 | 0.40 |
| 5/12 | 14.3 | 4.6 | 0.32 | 8.6 | 0.60 |
| 6 | 16.4 | 1.6 | 0.10 | 13.1 | 0.80 |
| 7/9 | 16.6 | 6.6 | 0.40 | 8.3 | 0.50 |
| 8 | 16.6 | 1.7 | 0.10 | 10.0 | 0.60 |
| 10 | 14.9 | 7.5 | 0.50 | 7.5 | 0.50 |
| 11 | 14.5 | 3.3 | 0.23 | 8.7 | 0.60 |
| CV ¹ | | 0.53 | 0.63 | 0.23 | 0.30 |

¹ Coefficient of variation (standard deviation divided by the mean) over all chromosomes.